

PAPER • OPEN ACCESS

Highly symmetric and tunable tunnel couplings in InAs/InP nanowire heterostructure quantum dots

To cite this article: Frederick S Thomas *et al* 2020 *Nanotechnology* **31** 135003

View the [article online](#) for updates and enhancements.

Recent citations

- [Electrical probing of carrier separation in InAs/InP/GaAsSb core-dualshell nanowires](#)
Sedighe Salimian *et al*
- [Controlled Quantum Dot Formation in Atomically Engineered Graphene Nanoribbon Field-Effect Transistors](#)
Maria El Abbassi *et al*
- [Orbital Tuning of Tunnel Coupling in InAs/InP Nanowire Quantum Dots](#)
Zahra Sadre Momtaz *et al*






IOP | ebooks™

Bringing together innovative digital publishing with leading authors from the global scientific community.

Start exploring the collection—download the first chapter of every title for free.

Highly symmetric and tunable tunnel couplings in InAs/InP nanowire heterostructure quantum dots

Frederick S Thomas^{1,5} , Andreas Baumgartner^{1,2,5}, Lukas Gubser^{1,2}, Christian Jünger¹, Gergő Fülöp¹, Malin Nilsson¹, Francesca Rossi³ , Valentina Zannier⁴ , Lucia Sorba⁴ and Christian Schönenberger^{1,2}

¹ Department of Physics, University of Basel, Klingelbergstrasse 82, CH-4056 Basel, Switzerland

² Swiss Nanoscience Institute, University of Basel, Klingelbergstrasse 82, CH-4056 Basel, Switzerland

³ IMEM—CNR, Parco Area delle Scienze 37/A, I-43124 Parma, Italy

⁴ NEST, Istituto Nanoscienze—CNR and Scuola Normale Superiore, Piazza San Silvestro 12, I-56127 Pisa, Italy

E-mail: frederick.thomas@unibas.ch and andreas.baumgartner@unibas.ch

Received 17 September 2019, revised 8 November 2019

Accepted for publication 28 November 2019

Published 13 January 2020



CrossMark

Abstract

We present a comprehensive electrical characterization of an InAs/InP nanowire (NW) heterostructure, comprising of two InP barriers forming a quantum dot (QD), two adjacent lead segments and two metallic contacts. We demonstrate how to extract valuable quantitative information of the QD. The QD shows very regular Coulomb blockade resonances over a large gate voltage range. By analyzing the resonance line shapes, we map the evolution of the tunnel couplings from the few to the many electron regime, with electrically tunable tunnel couplings from $<1 \mu\text{eV}$ to $>600 \mu\text{eV}$, and a transition from the temperature to the lifetime broadened regime. The InP segments form tunnel barriers with almost fully symmetric tunnel couplings and a barrier height of $\sim 350 \text{ meV}$. All of these findings can be understood in great detail based on the deterministic material composition and geometry. Our results demonstrate that integrated InAs/InP QDs provide a promising platform for electron tunneling spectroscopy in InAs NWs, which can readily be contacted by a variety of superconducting materials to investigate subgap states in proximitized NW regions, or be used to characterize thermoelectric nanoscale devices in the quantum regime.

Keywords: InAs/InP, nanowire, quantum dot, tunnel barrier, electron tunneling spectroscopy, coulomb resonance line shape


(Some figures may appear in colour only in the online journal)

1. Introduction

Semiconducting nanowires (NWs), such as InAs or InSb NWs, have recently attracted significant attention, for example as

building blocks in topological quantum computation [1], sources of entangled electrons [2, 3], spintronics [4], or thermoelectrics [5]. Fundamental unique properties of these systems are their strong spin–orbit interaction [6, 7], large and tunable g -factors [8, 9], and are an excellent thermoelectric figure of merit (ZT) [10]. These properties make them promising material platforms for various scalable electronic devices, as well as for investigating fundamental physics on the nanometer scale. Significant progress has been made in the synthesis and band-structure engineering of III–V semiconductors. For example, quantum dots (QDs) can be embedded into radial [11, 12] and

⁵ Authors to whom any correspondence should be addressed.

 Original content from this work may be used under the terms of the [Creative Commons Attribution 3.0 licence](https://creativecommons.org/licenses/by/3.0/). Any further distribution of this work must maintain attribution to the author(s) and the title of the work, journal citation and DOI.

axial [13–15] NW heterostructures, directly grown complex multiple NW geometries such as crosses [16–18] or networks [19] have become feasible, as well as *in situ* grown epitaxial superconducting shells [20] for superconducting hybrid devices [21, 22].

Several theoretical proposals suggest using semiconductor-superconductor NW hybrid systems to artificially create exotic quantum states of matter, such as Majorana bound states [23–25], and to read out qubit states [26, 27]. NW heterostructures with *in situ* grown tunnel barriers are a promising platform to bring such experiments to the next level of control and to a quantitative understanding. To obtain a reliable spectroscopic tool, QDs with systematically tunable characteristics are essential. In contrast to electrostatic gating [28], this can be achieved using *in situ* grown tunnel barriers in InAs NWs, either by modifying the crystal phase [29] or by introducing a larger band gap material such as InP [30]. Crystal-phase defined double barriers in InAs NWs result in stable and well controllable QDs [29], and were recently used to probe the evolution of the superconducting proximity gap in an adjacent NW segment [31]. However, the relatively low and long tunnel barriers [32, 29] limit the spectroscopic range, while the large carrier concentrations in the zinc-blende sections make studies of few mode quantum systems challenging.

Here, we use InAs/InP NW heterostructure QDs, where a QD is formed between two InP segments in a wurtzite InAs NW. These *in situ* grown tunnel barriers result in a strong confinement due to a large conduction band edge offset of $V_0 \approx 400\text{--}600$ meV between the InAs and the InP segments [33, 34]. Similar heterostructures have been used previously to investigate single [30, 35, 36] and double [37, 38] QD physics, as well as thermoelectric transport [10].

We present an in-depth analysis of an InAs/InP heterostructure QD demonstrating their exceptional long term stability and broad electrical tunability. We report a detailed and comprehensive characterization of the InP tunnel barriers and the resulting Coulomb blockade (CB) resonance lineshapes, which can be crucial, for example, to distinguish different single electron [39] or superconducting subgap transport processes [3, 40]. We show that the *in situ* grown InP barriers result in highly predictable, electrically tunable, and symmetric QDs with level broadenings that are small enough for high resolution spectroscopy of subgap states in hybrid systems, demonstrated by distinct spectral features in the lead segments (LSs).

2. Results

2.1. Device fabrication

The InAs/InP heterostructure NWs were grown by gold assisted chemical beam epitaxy [15] and have a diameter of 50 ± 5 nm, depending on the size of the gold seed particle. The QD is formed on an InAs segment of length $s \approx 19$ nm, bounded by two InP barriers of width $\ell_1, \ell_2 \approx 5.5$ nm, as shown in figure 1. The dimensions of the InP barriers were determined in a transmission electron microscopy (TEM)

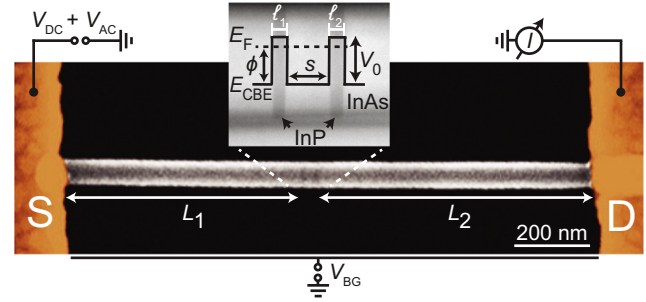


Figure 1. False colored scanning electron micrograph of a typical device consisting of an InAs nanowire with two *in situ* grown InP tunnel barriers of length $\ell_1, \ell_2 \approx 5.5$ nm. The nanowire segments between the contacts (S/D) and the quantum dot (QD) are referred to as the lead segments LS_{1/2} of lengths $L_{1/2}$. A QD of length $s \approx 19$ nm forms between the two tunnel barriers due to the conduction band offset, V_0 , between InAs and InP. V_{BG} is the global backgate voltage that simultaneously tunes the QD and the LSs. The inset shows a transmission electron microscopy image of two InP segments pointed out by two black arrows and an energy diagram of the gate tunable conduction band edge, E_{CBE} . The Fermi energy, E_F , is indicated by a dashed line and the difference between E_F and E_{CBE} is defined as ϕ .

analysis of NWs of the same growth. The device was fabricated on a degenerately p-doped silicon substrate acting as a global back gate with a 400 nm thick SiO₂ capping layer. The electrical contacts to the NW are made of titanium/gold films with a thickness of 5 nm/65 nm. Before evaporating the contact material, the native oxide of the NWs is etched with an (NH₄)₂S_x:H₂O solution [41]. A false color scanning electron microscopy (SEM) image of a typical device is shown in figure 1. In contrast to crystal-phase defined InAs QDs, the two InP segments can be imaged directly by standard SEM techniques with an in-lens detector [29].

We explicitly refer to the regions of bare InAs between the QD and the source or drain contact as the LSs. The lead segment LS₁ between the QD and the source contact is $L_1 \approx 350$ nm long, while the lead segment LS₂ between the QD and the drain contact is $L_2 \approx 600$ nm long. The QD and the LSs are tuned simultaneously by the back gate voltage V_{BG} , which shifts the conduction band edge, $E_{CBE}(V_{BG})$, relative to the Fermi energy, E_F , to higher or lower values. For later, we use $\phi(V_{BG}) = E_F - E_{CBE}(V_{BG})$.

The inset of figure 1 shows a TEM image of the epitaxially defined QD region in a similar NW. The two InP segments, indicated by black arrows, act as tunnel barriers with a rectangular potential profile for electrons due to the atomically sharp transitions in the material composition. The barrier height depends the band gap discontinuities and residual strain. For our NW geometry, the barrier height is predicted to be $V_0 \approx 400$ meV [34], providing a strong confinement to the electrons in the axial direction.

All measurements were performed in a dilution refrigerator with a base temperature of ~ 30 mK. We apply a DC voltage to the source electrode to correct for small offsets ($V_{DC} \approx 50 \mu\text{V}$) and superimpose an AC voltage of typically $1 \mu\text{V}_{\text{rms}}$ for lock-in detection, while the drain electrode is

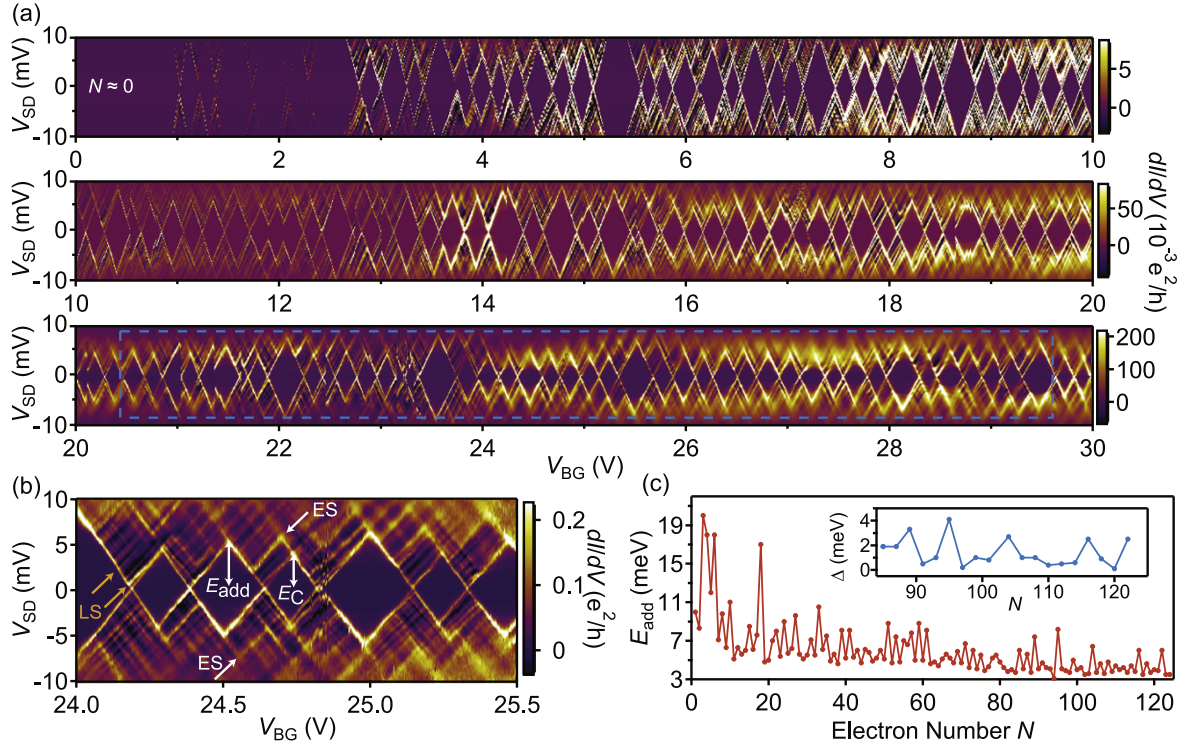


Figure 2. Differential conductance, dI/dV_{SD} , as a function of the bias, V_{SD} , and the back gate voltage, V_{BG} . (a) Regular and stable Coulomb diamonds over a gate range of 30 V, ranging from near depletion with an electron population of approximately zero ($N \approx 0$) to $N = 124$. (b) High resolution Coulomb diamonds, where excited state (ES) resonances of the QD and the resonances due to a modulation in the density of states in the semiconducting lead segments (LSs) are pointed out by white and orange arrows, respectively. (c) The addition energy, E_{add} , as a function of the number of electrons on the quantum dot, N . The inset shows the difference of single particle energy spacing, Δ , as a function of N in the many electron regime extracted from the region indicated by the blue box in (a).

grounded and used for the current (I) measurement. The differential conductance $dI/dV_{SD} = I_{AC}/V_{AC}$ was measured using standard lock-in techniques.

2.2. Characterization of the QD

Figure 2(a) shows dI/dV_{SD} as a function of V_{SD} and V_{BG} . We observe regular, stable, and reproducible Coulomb diamonds (CDs) over the large backgate range of 30 V, corresponding to the addition of ~ 124 electrons. At $V_{BG} \approx 1$ V, the number of electrons on the QD is close to zero, i.e. $N \approx 0$. By increasing V_{BG} , electrons are added to the QD sequentially, which brings the QD into the many electron regime. For the measurement sequence shown in figure 2(a), the maximum number of electrons on the QD is $N \approx 124$. When increasing V_{BG} beyond 40 V, thermal activation of carriers across the tunnel barriers begins to considerably contribute to the transport.

According to the constant interaction model [42], assuming two-fold spin-degenerate orbitals, the energy required to add an electron to a QD with an even electron configuration is given by the addition energy $E_{add} = E_C + \Delta$, with $E_C = e^2/C_\Sigma$ the charging energy, the total capacitance C_Σ of the QD, and Δ the single particle energy spacing. To add a second electron to the same QD orbital requires $E_{add} = E_C$. This gives rise to an alternating even-odd pattern of large and small CDs, characteristic for spin-degenerate QD states, and allows one to extract the corresponding energy scales. A region of the CDs shown in figure 2(b) exhibits a clear even-odd pattern with

$E_{add} = 5.5$ meV and $E_C = 4.2$ meV, as indicated by the white arrows. From the difference between E_{add} and E_C , we find $\Delta = 1.3$ meV, consistent with $\Delta \approx 1.6$ meV from the corresponding excited state (ES) resonances outside the CDs, pointed out by white arrows.

In figure 2(c) we plot E_{add} as a function of N for the full V_{BG} range of figure 2(a). We find an overall decrease in $E_{add}(N)$ for increasing N due to changes in the QD capacitance by electron-electron interactions [43]. From the very regular even-odd pattern in the gate range indicated by the blue box in figure 2(a), we extract $\Delta(N)$, as shown in the inset of figure 2(c). We find that Δ strongly scatters and assumes values in between 0.2 and 4 meV, suggesting that only single levels contribute to the transport.

In addition to the QD ES resonances, we find several other features outside of the CDs that cannot be attributed to the energy spectrum of the QD. For example, the resonances indicated by orange arrows in figure 2(b) are due to a non-constant DOS in the LSs, forming as standing waves in the LSs. Since these waves are strongly reflected at the InP barrier, the widths of these states are determined mostly by the coupling to the source and drain contacts, respectively. In addition, we find negative differential conductance (NDC) throughout the entire gate range, which we attribute to the simultaneous tuning of the QD and the LSs with different lever arms. We note that the NDC is more prominent in the few electron regime where the carrier concentration is low.

The NDC supports our notion that the DOS in the LSs is not constant, which is typical for NW QD devices with semiconductor leads [30].

2.3. Resonance line shapes

In this section, we extract the total tunnel coupling of the QD, Γ , and the electron temperature in the LSs, T , from the CB resonances. The total tunnel coupling, $\Gamma = \Gamma_1 + \Gamma_2$, is given by the individual couplings to the source and drain leads, Γ_1 and Γ_2 . In the case of an ideal measurement setup, the line shape only depends on Γ , T [44], and the asymmetry $A = \Gamma_1/\Gamma_2 \geq 1$ [45, 46]. However, there are also extrinsic broadening mechanisms, such as noise in the source and drain contacts, and on the gate, as well as the applied AC voltage.

For our analysis, we assume that only a single QD level contributes to the transport, i.e. eV_{AC} , Γ , $4k_B T \ll \Delta$ ⁶, and account for the three main broadening contributions: V_{AC} , Γ , and T . V_{AC} limits the smallest width of the line shape that can be reliably extracted, therefore eV_{AC} should be chosen such that $eV_{AC} < 4k_B T$, Γ . By tuning E_{CBE} with V_{BG} , we can access three different regimes: thermally broadened (Γ , $eV_{AC} \ll 4k_B T$), lifetime broadened ($4k_B T$, $eV_{AC} \ll \Gamma$), or a combination of both ($eV_{AC} \ll \Gamma \approx 4k_B T$). These three regimes are summarized in figures 3(a), (c), and (e), where the lifetime broadening is indicated by the width of the blue QD levels and the thermal broadening by the width of the orange Fermi–Dirac distribution in the LSs.

We model the line shape of the CB resonances with the assumption that the DOS in the LSs is constant and discuss effects due to a non-constant DOS later. For a single energy level, the line shape of a conductance resonance is described by a resonant tunneling model [44, 47, 48]:

$$I = g \frac{e}{h} \int T_{QD}(E) [f_S(E) - f_D(E)] dE, \quad (1)$$

where $g = 1$ is the number of independent parallel transport channels, $T_{QD}(E) = (\Gamma_1 \Gamma_2) / (\Delta E^2 + \Gamma^2/4)$ the Breit–Wigner (BW) transmission function [47] with $\Delta E = E - E_0$ the detuning from the CB resonance centered at E_0 , and $f_{S/D}(E) = 1 / (1 + \exp((E + eV_{S/D})/k_B T))$ are the Fermi–Dirac distributions in the LSs. dI/dV is calculated numerically. The contribution of V_{AC} is accounted for by evaluating equation (1) for a sinusoidal V_S that also electrically gates the QD. If not chosen properly, V_{AC} can mask the ‘true’ resonance and the measured resonance width is then given by V_{AC} .

In the regime where the broadening is mainly due to temperature, $\Gamma \ll 4k_B T \ll \Delta$, equation (1) reduces to $G/G_{max} = \cosh^{-2}(\Delta E/2k_B T)$, where $G_{max} = e^2/h \cdot \pi / (2k_B T) \cdot (\Gamma_1 \Gamma_2 / \Gamma)$ [44]. In this limit, T can be extracted from the full-width at half maximum (FWHM) of the resonance by $FWHM \approx 3.5k_B T$.

In the limit, where the broadening is mainly due to the electron lifetime on the QD, $4k_B T \ll \Gamma \ll \Delta$, equation (1) reduces to the BW formula [47] $G/G_{max} = (\Gamma/2)^2 / (\Delta E^2 + (\Gamma/2)^2)$ with $G_{max} = e^2/h \cdot 4\Gamma_1 \Gamma_2 / \Gamma^2$. In this limit, $FWHM =$

⁶ $4k_B T$ is the 10%–90% width of the Fermi–Dirac distribution.

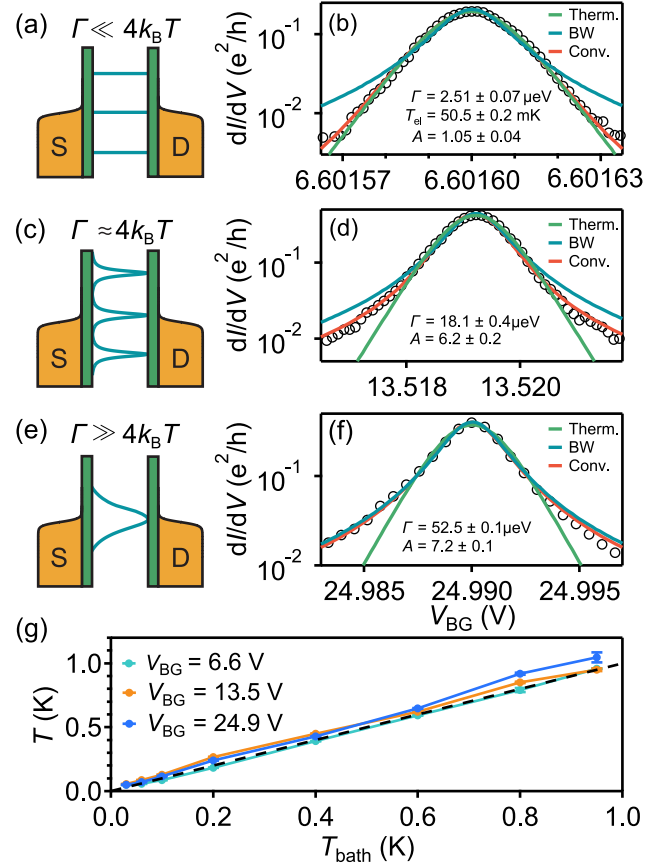


Figure 3. Differential conductance dI/dV as a function of V_{BG} for three resonances (b), (d), (f) in different regimes: (a) $\Gamma \ll 4k_B T$, (c) $\Gamma \approx 4k_B T$, and (e) $\Gamma \gg 4k_B T$. From (b), the electron temperature, $T = 50.5 \pm 0.2$ mK, was extracted and was fixed in the fits of (d) and (f). (g) T as a function of the bath temperature, T_{bath} , of the three resonances in (b), (d) and (f), respectively. T remains constant for $T_{bath} < 60$ mK, then increases with a slope of 1.00 ± 0.05 , as expected for the thermally broadened regime.

Γ and A determines the maximum conductance $G_{max} = e^2/h \cdot 4A/(1+A)^2$.

2.4. Evolution of the resonance line shapes

We now investigate how the line shapes of the resonances evolves with V_{BG} and the bath temperature, T_{bath} . Figures 3(b), (d), and (f) show high resolution CB resonance measurements in the three broadening regimes. To show the evolution of Γ , each of the three CB resonances was fit with the expressions for a thermal, BW, and the convolution line shape, described by equation (1). From the convolution fit, we extract Γ_1 , Γ_2 , T , and their corresponding standard error of the individual fits, shown as error bars in figures 3(g) and 4.⁷

Figure 3(b) shows a CB resonance near depletion ($N \approx 10$) at $V_{BG} = 6.6$ V, measured with $V_{AC} = 0.1 \mu V$. The convolution line shape agrees very well with the experiment, as does the pure thermal broadening line shape, but not the BW line shape. In this regime, the conduction band edge of the LSs is near the Fermi

⁷ This error bar does not account for potential experimental errors in consecutive experiments.

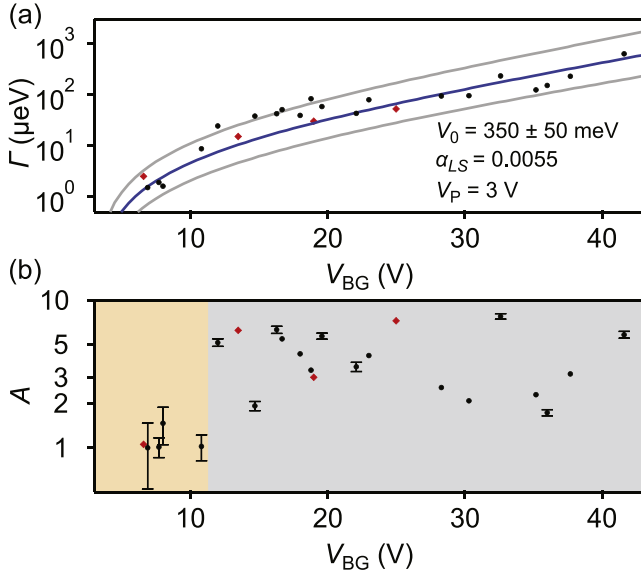


Figure 4. (a) Total tunnel coupling Γ as a function of the back gate voltage, V_{BG} . Γ systematically increases with V_{BG} in agreement with a double barrier model described in the main text. We estimate a conduction band edge offset, V_0 , between InAs and InP of 350 ± 50 meV (solid blue line), while the upper and lower solid gray lines are for $V_0 = 400$ meV and $V_0 = 300$ meV, respectively. (b) Asymmetry, $A = \Gamma_1/\Gamma_2$, as a function of V_{BG} . For low V_{BG} , $A \approx 1$, while for larger V_{BG} A scatters between 1 and 8. The red data points were extracted from the CB resonances in figures 3(b), (d), and (f) measured with a higher V_{BG} resolution than the black data points. Error bars smaller than the symbol size are not shown.

level ($\phi \ll V_0$) and the electrons are strongly confined by the large tunnel barriers, such that the width of the Coulomb resonance is mostly determined by the electron temperature and not by the QD lifetime. Only in this regime, we can accurately determine the electron temperature of the LSs. From the convolution fit, the extracted total tunnel coupling, asymmetry, and electron temperature are $\Gamma = 2.51 \pm 0.07 \mu\text{eV}$, $A = 1.05 \pm 0.04$, and $T = 50.5 \pm 0.2$ mK, respectively. We see that T is somewhat higher than the bath temperature ($T_{\text{bath}} = 30$ mK), probably due to noise and radiation due to insufficient filtering. Since T is not expected to change with V_{BG} , we set $T = 50.5$ mK for the following analysis of data at the same T_{bath} .

For the resonance at $V_{BG} = 13.5$ V ($N \approx 50$) a transition from the thermally to the lifetime broadened regime begins. As shown in figures 3(c) and (d), only the convolution line shape fits the data well. From the convolution fit, with $T = 50.5$ mK and $V_{AC} = 0.25 \mu\text{V}$ fixed, $\Gamma = 18.1 \pm 0.4 \mu\text{eV}$ and $A = 6.2 \pm 0.2$ were extracted from the fit. Therefore, this resonance is in the regime where the lifetime and thermal broadening contributes equally significantly with $\Gamma \approx 4k_B T$.

By increasing the gate voltage further, the CB resonances transition into the lifetime broadened regime with $\Gamma \gg 4k_B T$. This can be seen for the resonance in figure 3(f) at $V_{BG} = 24.99$ V ($N \approx 100$), where the data agrees very well with the convolution fit, as well as with the BW fit, with $T = 50.5$ mK and $V_{AC} = 1 \mu\text{V}$ fixed. From the convolution fit, we extract $\Gamma = 52.5 \pm 0.1 \mu\text{eV}$ and $A = 7.2 \pm 0.1$,

which shows that the resonance is mostly lifetime broadened ($\Gamma \gg 4k_B T$).

For each of the three resonances, the temperature dependence of the CB resonances was investigated, as shown in figure 3(g). We used the convolution fit with Γ_1 and Γ_2 fixed at the values determined at $T_{\text{bath}} = 30$ mK, to extract T for a series of different T_{bath} . For low T_{bath} , the CB resonances are either thermally broadened for $\Gamma \ll 4k_B T$, lifetime broadened for $4k_B T \ll \Gamma$, or a combination of the two for $\Gamma \approx 4k_B T$, as discussed in the previous section. For bath temperatures between 30 and 60 mK, the extracted T remains constant. As we increase T_{bath} beyond 60 mK, T for two resonances (cyan and orange) increases with a slope of 1.00 ± 0.05 , in agreement with the thermally broadened regime. This is indicated by the dashed black line with a slope of 1. However, for the blue resonance, which is mostly lifetime broadened, the slope is 1.2 ± 0.1 , likely due to the resonance not fully transitioning into the temperature broadened regime. These experiments show that the electron and phonon system equilibrate at ~ 100 mK and that InAs/InP heterostructure QDs can be used as *in situ* thermometers. In contrast to typical CB thermometers [49, 50], integrated QDs form an integral part of the device, which does not require thermal coupling to a separate device. We note that a series of thermal cycling takes roughly one week during which we did not observe any charge rearrangements, demonstrating a unique stability of this type of QD. Only tuning V_{BG} on the scale of several tens of volts results in a shift of the CB spectrum, which is reproducible and likely due to significant charging of substrate states.

2.5. Properties of the tunnel barriers

By investigating the functional dependence of the total tunnel coupling Γ and the asymmetry A on V_{BG} , we estimate the height and symmetry of the tunnel barriers formed by the InP segments. By fitting the CB resonances with equation (1) and using the previously determined $T = 50.5$ mK, we extract Γ and A as a function of V_{BG} , as shown in figures 4(a) and (b), respectively. The red data points correspond to the CB resonances from figures 3(b), (d), and (f) measured with a high resolution in V_{BG} , while the black data points stem from resonances selected from a large gate sweep ($\Delta N \approx 150$) over 50 V measured with a lower resolution.

$\Gamma(V_{BG})$ is plotted in figure 4(a) and shows a systematic increase of Γ with increasing V_{BG} . Close to full depletion, we find a tunnel coupling of $\Gamma \approx 1 \mu\text{eV}$, which increases up to $\sim 600 \mu\text{eV}$ for $V_{BG} = 42$ V. Comparing the dependence of $\Gamma(V_{BG})$ to a resonant tunneling model allows us to estimate V_0 . For this, we assume that an electron bounces back and fourth in the InAs segment between the two InP barriers at an attempt frequency ν and escapes through either of the barriers with a probability given by the rectangular tunnel barriers. Consequently, the total tunnel coupling Γ as a function of V_{BG} can be described by [51]:

$$\Gamma(V_{BG}) = 2\hbar\nu \left(1 + \frac{V_0^2 \sinh^2(\kappa(\phi)L)}{4\phi(V_0 - \phi)} \right)^{-1}, \quad (2)$$

with $\kappa(\phi) = \sqrt{2m_{\text{InP}}(V_0 - \phi(V_{\text{BG}}))/\hbar^2}$, $m_{\text{InP}} = 0.08m_e$ the effective electron mass in the InP segments [52], $\phi(V_{\text{BG}}) = e\alpha_{\text{LS}}(V_{\text{BG}} - V_{\text{P}})$, α_{LS} the lever arm of the LSs, V_{P} the pinch-off gate voltage, $\nu = v_{\text{F}}/2s$ the attempt frequency with Fermi velocity $v_{\text{F}} = \sqrt{\frac{2\phi}{m_{\text{InAs}}}}$, and $m_{\text{InAs}} = 0.04m_e$ the effective electron mass in wurzite InAs [53]. The values for the length of the InP segments and the QD were taken from the TEM analysis, with $\ell = \ell_{1/2} = 5.5$ nm and $s = 19.0$ nm, respectively.

From the best fit of equation (2) to $\Gamma(V_{\text{BG}})$ (solid blue), we obtain the free parameters $V_0 = 350 \pm 50$ meV, $V_{\text{P}} = 3$ V, and $\alpha_{\text{LS}} = 0.0053$. V_0 is in good agreement with the calculated literature value of $V_0 = 400$ meV for strained InP in InAs NWs with our geometry [34]. The upper and lower solid gray lines are obtained using the same parameters and $V_0 = 300$ meV and $V_0 = 400$ meV, respectively. V_{P} agrees very well with the first CB resonances and α_{LS} is 4.5 times smaller than the lever arm to the QD, in qualitative agreement with the LSs being longer than the QD.

Next, we investigate the asymmetry A as a function of V_{BG} in figure 4(b). The values of A scatter seemingly random between 1 and 8 for $V_{\text{BG}} > 10.5$ V. However, for $V_{\text{BG}} < 10.5$ V, $A \approx 1$ is constant, indicating highly symmetrical tunnel barriers. These characteristics of A can be understood qualitatively by the following argument. The modulation of the DOS in the confined LSs is determined by the single particle level spacing in the LSs, Δ_{LS} , and the broadening of the energy levels in the LSs, Γ_{LS} . At E_{F} , $\Delta_{\text{LS}} = \pi\hbar v_{\text{F}}/L_{1/2}$ for a parabolic dispersion relation and thus $\Delta_{\text{LS}} \sim \Delta/10$. In addition, the strong coupling between the LSs and the source or the drain contact gives rise to a larger Γ_{LS} than for the QD. With increasing V_{BG} , v_{F} also increases and we suspect that for $V_{\text{BG}} > 10.5$ V, $\Delta_{\text{LS}} > \Gamma_{\text{LS}}$, leading to a weaker overlap between the energy levels and thus to a stronger modulation of the DOS in the LSs. In contrast, for $V_{\text{BG}} < 10.5$ V, Δ_{LS} decreases and the energy levels in the LSs overlap stronger, resulting in a weaker modulation of the DOS. Consequently, in the low gate regime, A reflects the asymmetry of the tunnel barriers $A \approx 1$, which are essentially equal in length and height.

3. Summary and conclusion

In summary, we present an in-depth characterization of a QD formed by InP tunnel barriers and connected to metallic contacts via NW LSs. For this system we demonstrate a nearly depletible QD with CDs that are exceptionally robust against charge rearrangements over a large gate range of 30 V, corresponding to ~ 124 electron states, and several months measurement time. By analyzing the line shapes of the CB resonances, we find a continuous transition from the lifetime to the thermally broadened regime and extract the electron temperature in the LSs. The QD shows a systematic and tunable increase in the tunnel coupling, based on which we estimate the conduction band edge offset between the InAs and the InP segments as $V_0 = 350 \pm 50$ meV. The InP

segments act like ideal tunnel barriers with an asymmetry of $A = \Gamma_1/\Gamma_2 \approx 1$, as targeted in the crystal growth. This is found for low V_{BG} , where the modulation of the DOS in the LSs is negligible, while at larger V_{BG} the transport is modulated by the NW lead states. In conclusion, we demonstrate that integrated InAs/InP QDs are a promising platform for quantitative *in situ* electron tunneling spectroscopy and thermometry for future superconducting hybrid devices and other electronic and thermoelectrical applications.

Acknowledgments

The authors thank Raphaëlle Delagrange for fruitful discussions. This research was supported by the Swiss National Science Foundation through (a) a project Grant entitled ‘Quantum Transport in Nanowires’ Granted to CS (b) the National Centre of Competence in Research Quantum Science and Technology and (c) the QuantEra project SuperTop. It has further been supported by a PhD Grant from the Swiss Nanoscience Institut (SNI) and the University of Basel. This project has also received support from European Union’s Horizon 2020 research and innovation programme under Grant agreement No. 828948, project AndQC. The authors declare no competing financial interest. All data in this publication are available in numerical form at DOI: <https://doi.org/10.5281/zenodo.3417090>.

Author Contributions

FT fabricated the device and performed the measurements. FT, AB, MN, and GF analyzed the data. CJ supported the fabrication and performed several electrical characterization measurements on different growth batches of the InAs/InP NWs. LG fabricated, measured, and analyzed a similar device. GF performed measurements for a similar device that FT and CJ fabricated. FR, VZ, and LS developed the nanowire structure. CS and AB planned and designed the experiments, and participated in all discussions. All authors contributed to the manuscript.

ORCID iDs

Frederick S Thomas  <https://orcid.org/0000-0003-0576-546X>

Francesca Rossi  <https://orcid.org/0000-0003-1773-2542>

Valentina Zannier  <https://orcid.org/0000-0002-9709-5207>

References

- [1] Alicea J, Oreg Y, Refael G, von Oppen F and Fisher M P A 2011 *Nat. Phys.* **7** 412–7
- [2] Hofstetter L, Csonka S, Nygård J and Schönberger C 2009 *Nature* **461** 960–3
- [3] Fülöp G *et al* 2015 *Phys. Rev. Lett.* **115** 227003

- [4] Nadj-Perge S, Frolov S M, Bakkers E P A M and Kouwenhoven L P 2010 *Nature* **468** 1084–7
- [5] Karg S F, Troncale V, Drechsler U, Mensch P, Kanungo P D, Schmid H, Schmidt V, Gignac L, Riel H and Gotsmann B 2014 *Nanotechnology* **25** 305702
- [6] Kosaka H, Kiselev A, Baron F, Kim K W and Yablonovitch E 2001 *Electron. Lett.* **37** 464
- [7] Fasth C, Fuhrer A, Samuelson L, Golovach V N and Loss D 2007 *Phys. Rev. Lett.* **98** 266801
- [8] Björk M T, Fuhrer A, Hansen A E, Larsson M W, Fröberg L E and Samuelson L 2005 *Phys. Rev. B* **72** 201307
- [9] D'Hollosy S, Fábrián G, Baumgartner A, Nygård J and Schönenberger C 2013 *AIP Conf. Proc.* **1566** 359–60
- [10] Prete D, Erdman P A, Demontis V, Zannier V, Ercolani D, Sorba L, Beltram F, Rossella F, Taddei F and Roddaro S 2019 *Nano Lett.* **19** 3033–9
- [11] Jiang X, Xiong Q, Nam S, Qian F, Li Y and Lieber C M 2007 *Nano Lett.* **7** 3214–8
- [12] Nilsson M, Namazi L, Lehmann S, Leijnse M, Dick K A and Thelander C 2016 *Phys. Rev. B* **94** 115313
- [13] Björk M T, Ohlsson B J, Sass T, Persson A I, Thelander C, Magnusson M H, Deppert K, Wallenberg L R and Samuelson L 2002 *Nano Lett.* **2** 87–9
- [14] Dick K A, Thelander C, Samuelson L and Caroff P 2010 *Nano Lett.* **10** 3494–9
- [15] Zannier V, Rossi F, Ercolani D and Sorba L 2019 *Nanotechnology* **30** 094003
- [16] Gooth J, Borg M, Schmid H, Schaller V, Wirths S, Moselund K, Luisier M, Karg S and Riel H 2017 *Nano Lett.* **17** 2596–602
- [17] Plissard S R et al 2013 *Nat. Nanotechnol.* **8** 859–64
- [18] Krizek F, Kanne T, Razmadze D, Johnson E, Nygård J, Marcus C M and Krogstrup P 2017 *Nano Lett.* **17** 6090–6
- [19] Gazibegovic S et al 2017 *Nat. Mater.* **548** 434–8
- [20] Krogstrup P, Ziino N L B, Chang W, Albrecht S M, Madsen M H, Johnson E, Nygård J, Marcus C M and Jespersen T S 2015 *Nat. Mater.* **14** 400–6
- [21] Deng M T, Vaitiekėnas S, Prada E, San-Jose P, Nygård J, Krogstrup P, Aguado R and Marcus C M 2018 *Phys. Rev. B* **98** 085125
- [22] Vaitiekėnas S, Deng M T, Nygård J, Krogstrup P and Marcus C 2018 *Phys. Rev. Lett.* **121** 037703
- [23] Chevallier D, Szumniak P, Hoffman S, Loss D and Klinovaja J 2018 *Phys. Rev. B* **97** 045404
- [24] Gharavi K, Hoving D and Baugh J 2016 *Phys. Rev. B* **94** 155417
- [25] Deng M T, Vaitiekėnas S, Hansen E B, Danon J, Leijnse M, Flensberg K, Nygård J, Krogstrup P and Marcus C M 2016 *Science* **354** 1557–62
- [26] Plugge S, Rasmussen A, Egger R and Flensberg K 2017 *New J. Phys.* **19** 012001
- [27] Leijnse M and Flensberg K 2011 *Phys. Rev. B* **84** 140501
- [28] Heedt S, Otto I, Sladek K, Hardtdegen H, Schubert J, Demarina N, Läth H, Grützmacher D and Schäpers T 2015 *Nanoscale* **7** 18188–97
- [29] Nilsson M, Namazi L, Lehmann S, Leijnse M, Dick K A and Thelander C 2016 *Phys. Rev. B* **93** 195422
- [30] Björk M T, Thelander C, Hansen A E, Jensen L E, Larsson M W, Wallenberg L R and Samuelson L 2004 *Nano Lett.* **4** 1621–5
- [31] Jünger C, Baumgartner A, Delagrance R, Chevallier D, Lehmann S, Nilsson M, Dick K A, Thelander C and Schönenberger C 2019 *Commun. Phys.* **2** 76
- [32] Chen I J, Lehmann S, Nilsson M, Kivisaari P, Linke H, Dick K A and Thelander C 2017 *Nano Lett.* **17** 902–8
- [33] Björk M T, Ohlsson B J, Sass T, Persson A I, Thelander C, Magnusson M H, Deppert K, Wallenberg L R and Samuelson L 2002 *Appl. Phys. Lett.* **80** 1058–60
- [34] Niquet Y M and Mojica D C 2008 *Phys. Rev. B* **77** 115316
- [35] Romeo L, Roddaro S, Pitanti A, Ercolani D, Sorba L and Beltram F 2012 *Nano Lett.* **12** 4490–4
- [36] Cornia S, Rossella F, Demontis V, Zannier V, Beltram F, Sorba L, Affronte M and Ghirri A 2019 arXiv:1907.12324v2
- [37] Fuhrer A, Fröberg L E, Pedersen J N, Larsson M W, Wacker A, Pistol M E and Samuelson L 2007 *Nano Lett.* **7** 243–6
- [38] Rossella F, Bertoni A, Ercolani D, Rontani M, Sorba L, Beltram F and Roddaro S 2014 *Nat. Nanotechnol.* **9** 997–1001
- [39] Lindemann S, Ihn T, Bieri S, Heinzel T, Ensslin K, Hackenbroich G, Maranowski K and Gossard A C 2002 *Phys. Rev. B* **66** 161312
- [40] Gramich J, Baumgartner A and Schönenberger C 2015 *Phys. Rev. Lett.* **115** 216801
- [41] Suyatin D B, Thelander C, Björk M T, Maximov I and Samuelson L 2007 *Nanotechnology* **18** 105307
- [42] Kouwenhoven L P, Austing D G and Tarucha S 2001 *Rep. Prog. Phys.* **64** 701–36
- [43] Hirose K and Wingreen N S 1999 *Phys. Rev. B* **59** 4604–7
- [44] Beenakker C W J 1991 *Phys. Rev. B* **44** 1646–56
- [45] Stone A D and Lee P A 1985 *Phys. Rev. Lett.* **54** 1196–9
- [46] Büttiker M 1986 *Phys. Rev. B* **33** 3020–6
- [47] Ihn T 2009 *Semiconductor Nanostructures* (Oxford: Oxford University Press)
- [48] Foxman E B, McEuen P L, Meirav U, Wingreen N S, Meir Y, Belk P A, Belk N R, Kastner M A and Wind S J 1993 *Phys. Rev. B* **47** 10020–3
- [49] Pekola J P, Hirvi K P, Kauppinen J P and Paalanen M A 1994 *Phys. Rev. Lett.* **73** 2903–6
- [50] Palma M, Scheller C P, Maradan D, Feshchenko A V, Meschke M and Zumbühl D M 2017 *Appl. Phys. Lett.* **111** 253105
- [51] Ihn T 2009 *Semiconductor Nanostructures* (Oxford: Oxford University Press) p 347
- [52] Kim Y S, Hummer K and Kresse G 2009 *Phys. Rev. B* **80** 035203
- [53] De A and Pryor C E 2010 *Phys. Rev. B* **81** 155210